PCCP

PAPER

View Article Online
View Journal | View Issue

Cite this: *Phys. Chem. Chem. Phys.*, 2017, **19**, 31813

Debye ring diffraction elucidation of 2D photonic crystal self-assembly and ordering at the air–water interface†

N. L. Smith, A. Coukouma, S. Dubnik and S. A. Asher*

Received 19th October 2017,
Accepted 15th November 2017

DOI: 10.1039/c7cp07130b

rsc.li/pccp

We fabricate 2D photonic crystals (2DPC) by spreading a dispersion of charged colloidal particles (diameters = 409, 570, and 915 nm) onto the surface of electrolyte solutions using a needle tip flow method. When the interparticle electrostatic interaction potential is large, particles self-assemble into highly ordered hexagonal close packed (hcp) monolayers. Ordered 2DPC efficiently forward diffract monochromatic light to produce a Debye ring on a screen parallel to the 2DPC. The diameter of the Debye ring is inversely proportional to the 2DPC particle spacing, while the Debye ring brightness and thickness depends on the 2DPC ordering. The Debye ring thickness increases as the 2DPC order decreases. The Debye ring ordering measurements of 2DPC attached to glass slides track measurements of the 2D pair correlation function order parameter calculated from SEM micrographs. The Debye ring method was used to investigate the 2DPC particle spacing, and ordering at the air–solution interface of NaCl solutions, and for 2DPC arrays attached to glass slides. Surprisingly, the 2DPC ordering does not monotonically decrease as the salt concentration increases. This is because of chloride ion adsorption onto the anionic particle surfaces. This adsorption increases the particle surface charge and compensates for the decreased Debye length of the electric double layer when the NaCl concentration is below a critical value.

Introduction

2-Dimensional photonic crystals (2DPC) are two dimensional dielectric periodic materials that control the propagation of light.[1] 2DPC are commonly fabricated using colloidal nano- or meso-particles with a significant dielectric constant difference from that of the surrounding media. When the particle diameter is on the same order as the wavelengths of light, the individual particles will Mie scatter the incident light. For a colloidal crystal like the a 2DPC, visible light is scattered from a periodic array of particles, causing interference of the scattered waves.[2,3] Constructive interference of the scattered waves from the periodic lattice results in Bragg diffraction, which is analogous to X-ray diffraction from ordered atomic and molecular crystal structures.[4,5] For 2D Bragg diffraction, white light is scattered by particles in a periodic monolayer such that each wavelength is diffracted at a particular angle.[6] The forward diffracted light through a 2DPC film diffracts as a rainbow. The Mie scattering cross sections are large. Thus, these 2DPC diffract nearly all incident light into the Debye ring.

These periodic, optical materials have numerous applications such as sensing,[7–9] waveguiding,[10–12] and superhydrophobic and antifogging coatings.[13–15] Further, these periodic materials are useful for fabricating SERS substrates,[16] for Localized Surface Plasmon Resonance Spectroscopy substrates,[17] and for particle lithography.[18–20] There is intense interest in the development of methods to fabricate large area, highly ordered 2DPC.[18,21]

Nanoparticle 2D array self-assembly is the most commonly used technique to fabricate 2DPC. Alternatively, AFM nanolithographic techniques offer a high level of precision for fabricating 2DPC structures with few defects.[22] Unfortunately, lithography is slow and limited to fabricating small areas. Self-assembly has the advantage of being less expensive than lithography; it can fabricate much larger areas in less time. Many methods have been developed to self-assemble nanoparticles into hexagonal close packed (hcp) ordered arrays, including the needle tip flow (NTF) method (which has recently been called micro-propulsive injection),[10,23] spin coating,[24] the Langmuir–Blodgett technique[18,25,26] wet coating,[27] floating,[28,29] and evaporation induced self assembly.[30,31]

Each of the self-assembly methods constrain interparticle interactions such that a hexagonal close packed structure is the minimum free energy.[32] The interactions that determine particle ordering differ between the different self-assembly techniques. For example, solvent–substrate and particle–substrate interactions that impact ordering in evaporation induced self-assembly methods[16,33] do not significantly impact ordering for particles

Department of Chemistry, University of Pittsburgh, Pittsburgh, Pennsylvania, USA. E-mail: asher@pitt.edu

† Electronic supplementary information (ESI) available. See DOI: 10.1039/c7cp07130b

self-assembled at the air–water interface. The interparticle interactions are optimized for each different method to improve particle ordering to obtain large hcp crystal domains. Alternatively, post self-assembly methods to improve 2DPC order have also been investigated. Shinotsuka *et al.*[18] utilized ultrasonic annealing, or repeated compression cycles after self-assembly at the air–water interface to increase the 2DPC order through Oswald ripening of the colloidal crystal domains.

In this work, we investigated the self-assembly of charged colloidal particles at the air–water interface using the needle tip flow method.[23,34] Our objective was to control the 2DPC ordering by decreasing the electrostatic repulsions between particles by the addition of NaCl to the water subphase. We monitored the 2DPC particle spacing and ordering by using Debye ring diffraction of visible light.

Experimental

Materials

Sodium 4-vinylbenzenesulfonate, ammonium persulfate, 2,2′-azobis(2-methylpropionitrile), 1-propanol, and 2-hydroxyethyl methacrylate were acquired from Sigma Aldrich (≥90% purity) and used as received. Styrene was acquired from Sigma Aldrich and purified by column chromatography. Methanol (>99.8%) and sodium chloride (>99.5%) were acquired from Fischer Scientific and used as received.

Polymerization and characterization of monodisperse negatively charged polystyrene nanoparticles

Negatively charged PS nanoparticles with diameters of 915 nm were synthesized by dispersion polymerization using a procedure described by Zhang *et al.*[35] Negatively charged polystyrene nanoparticles with diameters of 570 nm and 409 nm were synthesized by emulsifier free emulsion polymerization using a procedure described by Reese *et al.*[36]

The weight percent of each PS particle dispersion was calculated by dividing the weight of dried particles by the original weight of the dispersion. The average particle diameter was determined by measuring the diameter of >150 particles in SEM micrographs using the National Institute of Health program, ImageJ. SEM micrographs of 2DPC were obtained using a JEOL 6390LV Scanning Electron Microscope.

PS water dispersions were cleaned by centrifuging the particles into a pellet (10 000 RPM for 10 min) then redispersing them in nanopure water at least three times before use. The final volume of water added to the PS particle pellet was adjusted so that the final concentration is 15 wt% PS particles in water. The zeta-potentials of the PS particles in nanopure water, or in 0.001, 0.01, 0.1 or 1 M NaCl solutions were measured on a Brookhaven Zeta-PALS instrument.

2DPC Fabrication using needle tip flow method

We fabricated the 2DPC by self-assembling charged colloidal nanoparticles on a water surface using our Needle Tip Flow (NTF) method[23] as shown in Fig. 1. The 15 wt% PS nanoparticle

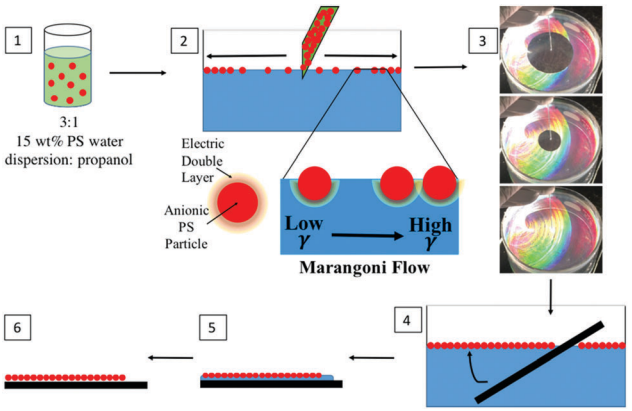

Fig. 1 Schematic of needle tip flow 2DPC fabrication at the air–water interface. (1) Addition of propanol lowers the surface tension of the particle dispersion. (2) The dispersion is spread on the water surface through a needle tip at a constant rate. The surface tension gradient forces the particles to the outer edge of the water surface. (3) The ESI† contains a video showing 2DPC self-assembly on the water surface. The boundary between the self-assembled 2DPC and the particle-free pure water surface is visually evident. The radius of this boundary decreases as more particles are spread onto the surface. (4) The 2DPC is lifted from the water surface by a microscope slide. (5) The wet slide with the lifted 2DPC is dried at room temperature. (6) After the water evaporation, the particles on the slide surface adhere to the microscope slide.

aqueous dispersion is mixed with propanol to lower the particle dispersion surface tension. The NTF flow method utilizes the Marangoni effect, which drives the PS particles to spread on the water surface due to surface tension gradients. The Marangoni flow guides the particles towards areas with higher surface tension, this directs particles towards the dish outer edge. Therefore, particles radially spread outwards from the needle tip to the edge of the water surface as shown in Fig. 1, part 3. The video provided in the ESI† demonstrates that the particles initially spread to cover the outer water surface at the edge of the dish.

A 21-gauge needle is attached to a 1 mL plastic syringe containing ~0.6 mL of a 3 : 1 PS particle dispersion: propanol mixture. A 9 cm diameter, 6 cm deep glass crystallization dish is filled with nanopure water, or aqueous salt solutions containing 0.001, 0.01, 0.1 or 1 M NaCl. The vertically oriented needle pierces the water surface such that half of the needle tip bevelled orifice bisects the water meniscus. The particle dispersion flow rate is controlled by the pressure applied to the 1 mL syringe plunger. The particle dispersion that is layered on the water surface spreads onto the water surface until the surface becomes completely covered with particles. Once the water surface is filled with the particle monolayer, the particle dispersion will begin to disperse into the bulk water instead of spreading on the surface. The circular boundary of the self-assembled 2DPC along the outer edge of the water surface is easily observed as shown in Fig. 1, part 3. The visually evident 2DPC boundary is monitored during particle deposition to determine the point when the water surface is filled with particles. The particle dispersion flowing onto the water surface is then stopped.

Optical microscopy was used to obtain images of a 2DPC made from 915 nm particles at the air–water interface. A Leica

TCS SP5 confocal laser scanning microscope with a Leica HCX-PL APO 40×/0.85 objective was used to collect images in transmission mode, and the scan rate was 100 Hz.

The 2DPC is lifted from the water surface with a glass microscope slide (Fig. 1, part 4). The slide is vertically inserted into the water. The plane of the slide is then rotated to be parallel with the water surface while the slide lifts the self-assembled 2DPC from the water surface. The slide is placed on a flat surface and allowed to dry at room temperature. After drying, the 2DPC adheres to the microscope slide surface. 2DPC were fabricated using 409, 570, and 915 nm diameter PS particles. The particles were self-assembled on nanopure water surfaces, and on aqueous salt solutions containing 0.001, 0.01, 0.1, and 1 M NaCl. Ten replicate samples were fabricated for each set of particles and salt solutions.

2DPC Debye ring diffraction measurements

The ordered 2DPC efficiently forward diffract light. In the case of a perfectly ordered 2DPC monochromatic light will be diffracted onto a screen parallel to the 2DPC monolayer as a hexagonal array of spots. These six spots correspond to the six reciprocal lattice vectors of the 2D close packed hexagonal particle array.

If the self-assembled 2DPC consists of small crystallites that are rotationally disordered, the diffraction of normal incident monochromatic light will form a continuous ring, called the Debye ring. We measured the Debye ring diameter to calculate the 2DPC particle spacing. We can utilize the Debye ring thickness to monitor the 2DPC order, provided that the width of the Debye ring is limited by disorder and not by the laser beam spot size.

For example, Fig. 2A shows the diffraction geometry used for measuring the Debye ring with a 406 nm violet laser diode (Thor Labs, 2.2 mm diameter spot size). The normally incident monochromatic light is forward diffracted at an angle, θ onto a screen parallel to the 2DPC plane. The diameter of the Debye ring projected onto the screen depends on both the 2DPC particle spacing, a and the distance, h between the 2DPC and the screen.

The Debye rings were measured at five different locations on each 2DPC attached to the glass slide. The difference between the outer and inner Debye ring diameters are the widths of the Debye rings. The average of the inner and outer diameters, d, gives us the Debye ring diffraction angle, θ (eqn (1)), and the particle spacing, a (eqn (2)).[7,37]

$$\theta = \tan^{-1}\frac{d}{2h} \quad (1)$$

$$a = \frac{2\lambda}{\sqrt{3}\sin\theta} \quad (2)$$

The Debye ring diffraction was also measured for a 915 nm 2DPC on the water surface. The measurements were repeated at least three times for the 2DPC on a nanopure water surface, and on 0.01 M, and 0.1 M NaCl solutions. The Debye rings were also measured for the 2DPC on the surface of the microscope slide directly after the 2DPC was lifted off the water surface.

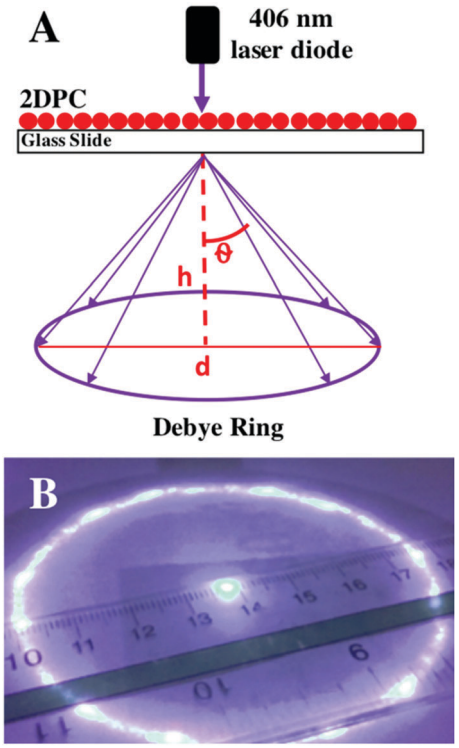

Fig. 2 (A) Debye ring measurements. A violet laser pointer (406 nm, 2.2 mm spot size) illuminates the 2DPC at normal incidence. The 2DPC diffracts the light, producing a Debye ring on the screen below. The diffraction angle, θ is calculated from the Debye ring diameter, d using $\tan(\theta) = d/2h$. (B) Photograph of the Debye ring diffraction of a 2DPC fabricated with 915 nm diameter particles.

As shown in Fig. 3 the diffraction of the 2DPC lying on the water surface is shifted due to refraction of the light by the air–water interfaces. The Debye ring diameter of a 2DPC on the water surface will be smaller than that from an identical 2DPC on a glass slide.

The diffraction angle in air, θ_a can be calculated from Debye ring diffraction measurements of a 2DPC on a water surface using eqn (3), which details the impact of Snell's law, $\theta_w = \sin^{-1}\left(\frac{n_a \sin\theta_a}{n_w}\right)$. The thickness and refractive index of water and air layers are h_w, n_w, and h_a, n_a respectively.

$$\frac{d}{2} = h_w \tan\left(\sin^{-1}\left(\frac{n_a \sin\theta_a}{n_w}\right)\right) + h_a \tan\theta_a \quad (3)$$

2DPC ordering analysis

We examined the ordering of three 2DPC samples for each set of experimental conditions. We sputter coated the 2DPC on glass slides with gold for 90 s (30 mA current) using a PELCO SC-7 sputter coater. The gold coated 2DPC were imaged using a scanning electron microscope (JEOL 6390LV SEM). Five SEM micrographs were collected from different areas of each 2DPC sample. Representative SEM images for each particle diameter and salt concentration are provided in the ESI.† These 2DPC images were used to calculate the 2D pair correlation function,

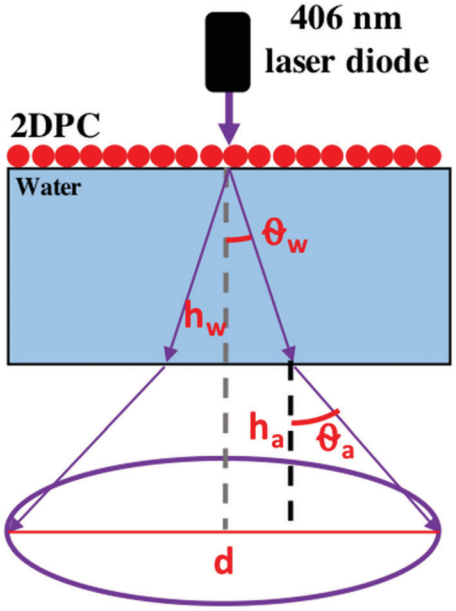

Fig. 3 Schematic showing the angles of diffraction for 406 nm light traveling through water, θ_w, and air, θ_a. The distance the light travels in each medium, h_w and h_a determines the final Debye ring diameter.

$g(r)$ (eqn (4)).[23,38,39] The pair correlation function calculates the number of particles (dn) within the area (da) of a ring having an inner diameter (r) and outer diameter (r + dr). $g(r)$ was calculated for shell radii ranging from 0 to 14, where dr was $0.016R_0$. R_0 is the particle radius and p is the particle number density.

$$g(r) = \frac{1}{\langle p \rangle} \frac{\mathrm{d}n(r, r+\mathrm{d}r)}{\mathrm{d}a(r, r+\mathrm{d}r)} \quad (4)$$

A detailed description of our 2DPC ordering analysis and the MATLAB code written to calculate the 2D pair correlation function can be found in the ESI.† Briefly, the MATLAB circle finding algorithm, imfindcircles, was used to find the centers of the particles in each SEM micrograph. This function creates a matrix of the particle positions from which the pair correlation function can be calculated. A discrete Fast Fourier Transform (FFT) was then calculated for the function $g(r) - 1$. The dimensionless order parameter, κ/κ_o is calculated as the ratio of the FWHM of the first FFT peak for a fabricated 2DPC, κ and the FWHM of the FFT peak for a perfect array, κ_o.[23] The average order parameter was calculated using data from at least 15 SEM micrographs for each experimental condition.

Results and discussion

Needle tip flow nanoparticle self-assembly at the air–water interface

The needle tip flow (NTF) method for self-assembling charged nanoparticles at the air–water interface produces highly ordered 2DPC, with large crystalline domains ($\sim$100 μm^2).[23,34] The 2DPC can be fabricated on large area water surfaces (730 cm^2 for a single needle tip) in $\sim$2 min using the NTF method (Fig. 1). Gao *et al.*[10] fabricated very large area ($\sim$1 m^2) 2DPC using a micro-propulsive injection method, which is analogous to our NTF method. They were able to quickly fabricate very large areas of 2DPC at the air–water interface because the particle dispersion was spread on the water surface at multiple injection points using syringe pumps.

The NTF flow method, described in previous papers[10,23,34,40,41] utilizes Marangoni flow that spreads the PS particle dispersion on the water surface. The Marangoni flow results from surface tension gradients that generate surface fluid motion such that lower surface tension liquid regions are pulled towards regions of high surface tension. The 15 wt% PS nanoparticle aqueous dispersion contains propanol to lower its surface tension. The resulting Marangoni flow spreads the particle dispersion radially outwards from the needle tip to the edge of the water surface (Fig. 1, part 3). As shown by the video in the ESI† the particles spread as a monolayer onto the surface until the entire water surface is covered.

The ordering of the self-assembled 2DPC depends on the rate of spreading and upon the detailed balance between attractive and repulsive particle interactions in the 2DPC film. Adding NaCl to the water subphase should decrease the electrostatic repulsions between these negatively charged particles.

This can be clearly shown by qualitatively viewing the 2DPC ordering in SEM micrographs as shown in Fig. 4a. 2DPC fabricated on higher concentration salt solutions are clearly less ordered. We can quantitatively determine the 2DPC order by calculating the 2D pair correlation function, $g(r)$, from these SEM micrographs.

Alternatively, we can quantitatively determine the 2DPC ordering without perturbing the sample by monitoring the Debye ring diffraction. Samples probed using the Debye ring diffraction

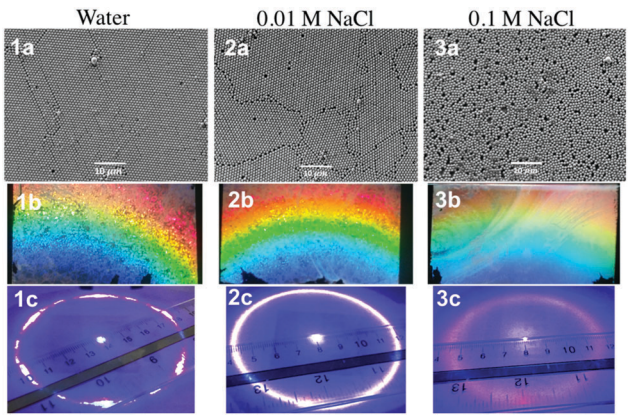

Fig. 4 SEM micrographs, a1 to a3, of 2DPC of 915 nm PS particles prepared on solutions of increasing salt concentrations (pure water, 0.01 M NaCl and 0.1 M NaCl). (b1–b3) Photographs of polychromatic light diffraction of 2DPC prepared on solutions of increasing salt concentrations. The polychromatic diffraction becomes more diffuse and less intense at larger salt concentrations. (c1–c3) Photographs of Debye ring diffraction of normally incident 405 nm monochromatic light at increasing salt concentrations. Debye ring diffraction photograph of the 2DPC at 0.1 M NaCl was edited with regards to brightness/contrast and color balance so that the Debye ring could easily be observed. This diffuse Debye ring is very hard to photograph because the weak diffraction intensity.

method can be used in future experiments, unlike samples that are sputtered with gold prior to SEM.

Estimating 2DPC order from Debye ring diffraction

Most of the light incident on the 2DPC is diffracted into the Debye ring.[42] Unlike for the case of 3D Bragg diffraction, 2DPC planes forward diffract polychromatic light such that each wavelength diffracts at a specific angle, θ as shown in Fig. 4.1b to 3b according to the 2D Bragg diffraction condition (eqn (5)) for a 2DPC particle array with spacing, a.

$$\lambda = \frac{\sqrt{3}a}{2}(\sin\alpha + \sin\theta) \quad (5)$$

For normally incident monochromatic light to the 2DPC plane, as shown in Fig. 2, $\sin\alpha = 0$, and eqn (5) becomes eqn (2). Thus, the light is forward diffracted at an angle, θ that depends on the particle spacing, a of the 2DPC array and the detailed 2DPC particle ordering. If a single 2DPC domain is irradiated, six spots are diffracted onto the screen (Fig. 4.1c). These six spots correspond to the six reciprocal lattice vectors of the 2D hcp particle array. The fabricated 2DPC studied here often show a distribution of randomly oriented 2D crystallites. Simultaneous irradiation of numerous crystalline 2DPC domains give rise to diffraction of a continuous Debye ring (Fig. 4.2c and 3c). The diameter of the Debye ring, determined by the diffraction angle θ, is inversely proportional to the 2DPC particle spacing, a.

Fig. 4 illustrates the impact of 2DPC disorder on the diffraction. The decreasing 2DPC ordering of the particle array self-assembled on water, 0.01 M NaCl, and 0.1 M NaCl is evident in the SEM micrographs in Fig. 4.a1–a3. As the 2DPC order decreases, the forward diffracted white light intensity decreases (Fig. 4.1b–3b), while the Debye ring thickness increases (Fig. 4.1c–3c). The Debye ring width (w), can be used to monitor the 2DPC order and particle spacing on the glass slides, as well as, at the air–water interface, without perturbing the 2DPC.

The disordered 2DPC Debye rings will be broader than Debye rings from highly ordered 2DPC. The disordered 2DPC Debye ring broadening results from variations of particle spacing within the probed areas as shown in Fig. 5. We are assuming the broadening contribution from the finite crystallite size is negligible compared to the laser beam spot size.

The hexagonal close packed (hcp) crystal shows the smallest plane spacing possible. This plane spacing will diffract light into the maximum diffraction angle for this particle diameter. The Debye ring width of a perfectly ordered close packed 2DPC is only limited by the incident laser spot size. Less ordered crystals will diffract light into smaller diffraction angles. The sum of these contributions broaden the Debye ring. The outer Debye ring diameter does not change because it is fixed at the minimum particle spacing of the 2DPC lattice. In contrast the Debye ring inner diameter will shrink with increasing disorder as the average particle spacing increases. In general, the standard deviations of the Debye ring measurements increase as the 2DPC disorder increases, because the particle spacing is more heterogeneous.

The Debye ring width and calculated particle spacing change of the 2DPC adhered to glass slides are shown in Fig. 6 and 7,

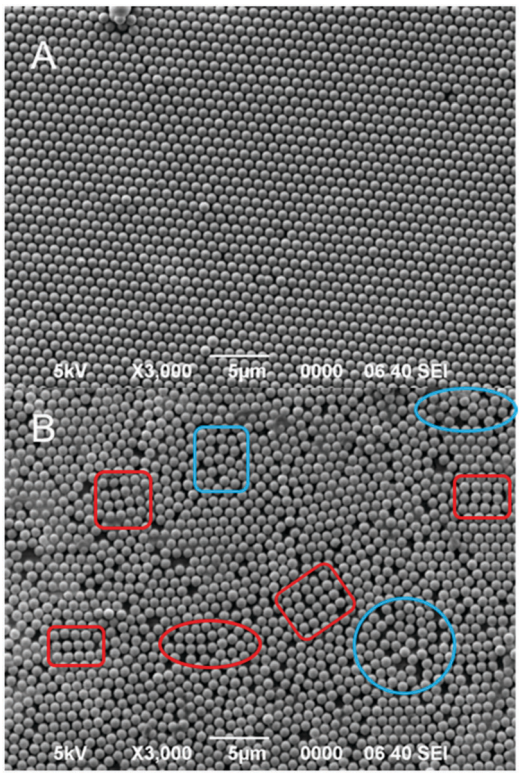

Fig. 5 SEM images of 915 nm particle 2DPC (A) self-assembled on pure water and (B) on 0.1 M NaCl. (A) Shows a well ordered 2DPC where the particle spacings show little variation. (B) Shows a highly disordered 2DPC. The areas outlined in red are where the particle arrays assembled into a square lattice instead of a hexagonal lattice. Areas highlighted in blue show regions that are randomly oriented with little crystalline order.

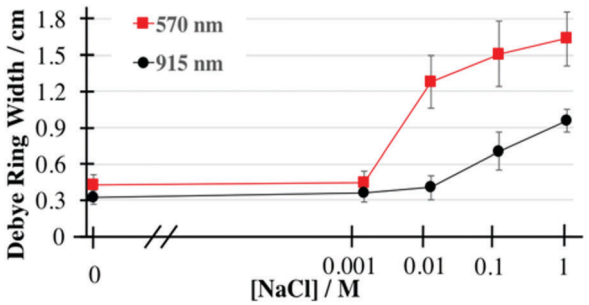

Fig. 6 Dependence of Debye ring widths of 570 nm and 915 nm 2DPC as a function of the NaCl concentration. Error bars represent one standard deviation.

respectively for 570 nm and 915 nm diameter particle arrays fabricated on water and on NaCl solutions. The particle spacings were calculated using eqn (1) and (2). The average of the inner and outer Debye ring diameter was used to calculate the average particle spacing.

The average salt induced particle spacing change is the difference between the particle spacing of the 2DPC fabricated on a salt solution and the particle spacing of the 2DPC fabricated on pure water, $\Delta a = a_{[\mathrm{NaCl}]} - a_{\mathrm{water}}$. The increasing particle spacing change results from the decreased inner diameter of the Debye ring.

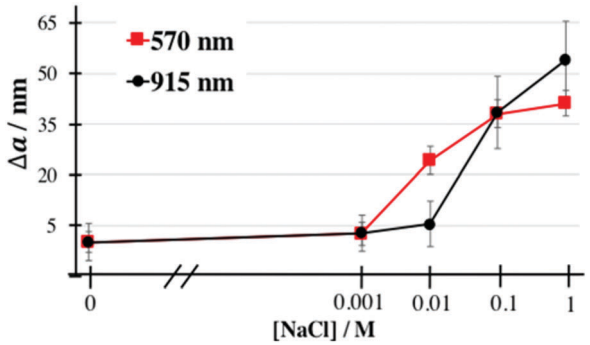

Fig. 7 Particle spacing change, $\Delta a = a_{[NaCl]} - a_{water}$, for 570 and 915 nm 2DPC as a function of NaCl concentration. Particle spacing is calculated from the Debye ring diameter measurements. Error bars represent one standard deviation.

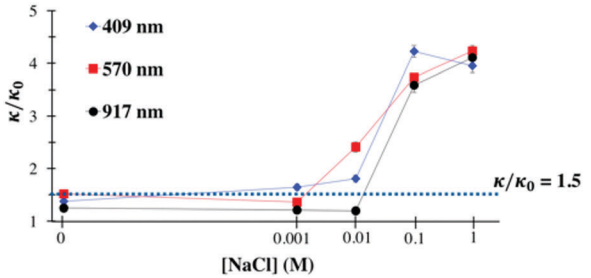

Fig. 8 Dependence of the 2DPC order parameter, κ/κ_o on salt concentration for 409, 570 and 915 nm particle diameters. The horizontal line indicates κ/κ_o = 1.5, above which significant disorder is present. Error bars indicate 95% confidence intervals.

We expect the Debye ring width to monotonically increase with NaCl concentration. The 2DPC ordering is determined by the balance of attractive and repulsive interactions between particles at the air–water interface.[21] The addition of salt to the water subphase should monotonically decease the electrostatic repulsions between particles. This leads to ''faster'' assembly of particle arrays because the probability of particle adhesion between colliding particles increases, leading to disordered particle aggregates that can serve as nucleation sites for crystal growth. The formation of randomly ordered particle clusters prevent 2D array annealing, where particles repel each other and arrange into a structure that minimizes the total energy of the system.

In contrast, our results indicate the 2DPC order is relatively unaffected by low concentrations of salt in the water subphase. The Debye ring width that is indicative of the 2DPC order, at low NaCl concentrations does not significantly differ from that of 2DPC fabricated in pure water. We find that there is a critical salt concentration, C^* of NaCl required to induce significant disorder. This critical salt concentration depends on the particle diameter, $C^* \approx$ 0.01 M NaCl for the 570 nm diameter particle 2DPC, while $C^* \approx$ 0.1 M NaCl for the 915 nm particle 2DPC.

We examined the salt concentration dependence of the order parameter, κ/κ_o from our measured 2D pair correlation function, $g(r)$ (eqn (4)) from SEM micrographs of the same samples used for our salt concentration Debye ring width measurements. We also studied 409 nm diameter particles to examine the dependence of the 2DPC ordering on the particle diameter.

The salt concentration dependence on the order parameter, κ/κ_o of the fabricated 2DPC, determined from the FFT of $(g(r) - 1)$, is shown in Fig. 8. The threshold for disorder occurs when $\kappa/\kappa_o > 1.5$.

The 2DPC order estimated from measurements of Debye ring width appears consistent with the detection of disorder from κ/κ_o calculated from SEM micrographs. The order parameter results confirm that 2DPC order does not significantly decrease until the salt concentration exceeds the critical salt concentration. Analogous to the Debye ring width results, C^* increases with an increasing particle diameter. The salt concentration at which $\kappa/\kappa_o > 1.5$ is 0.001 M NaCl for 409 nm diameter particles, 0.01 M for 570 nm particles, and 0.1 M NaCl for 915 nm particles. This dependence of the 2DPC ordering on the particle diameter and salt concentration is discussed below.

These results clearly indicate that the Debye ring width can be used to monitor the 2DPC order. This Debye ring width dependence is important because it enables non-destructive 2DPC order determinations of fragile systems such as the 2DPC at the air–water (or oil–water) interface.

2DPC ordering and particle spacing at the air–water interface

Three decades ago, Pieranski[43] showed that charged colloidal particles trapped at the air–water interface would self-assemble into ordered particle monolayers. Since then numerous additional methods were developed to fabricate close packed and non close packed ordered particle monolayers, and to transfer them onto solid substrates.[3,21,44,45] Each new method developed tuned the interparticle interactions to optimize the array ordering. Often, the ordering was monitored by determining the pair correlation function of images collected using electron microscopy[23,45,46] or AFM.[3] Any conclusions drawn from these SEM images must account for 2DPC disorder and particle spacing changes induced by transfer of the 2DPC from the air–water interface to the substrate and the impact of drying.

Optical microscopy has been used to investigate the particle array ordering at the air–water interface.[31,43,47] Confocal laser scanning microscopy is a powerful tool to investigate interfacial particle ordering, but the experiments require expensive optics and objectives. Confocal microscopy measurements are also complicated by motion of the air–water interface. In contrast, the Debye ring diffraction measurements allow us to easily probe the 2DPC ordering and particle spacing at the air–water interface using a laser pointer and a ruler or calliper.

The 2DPC particle spacing at the air–water interface is calculated from the Debye ring diameter using eqn (2) and (3). We also compared the spacings of the 2DPC transferred from these interfaces to wet and dry microscope slides. The post-transfer measurements were taken prior to evaporation of the thin water film on the microscope slide surface, where the particles are still trapped at this air–water interface. The Debye ring was also measured after slide water evaporation, where the 2DPC adheres to the slide. Fig. 9 shows the salt concentration

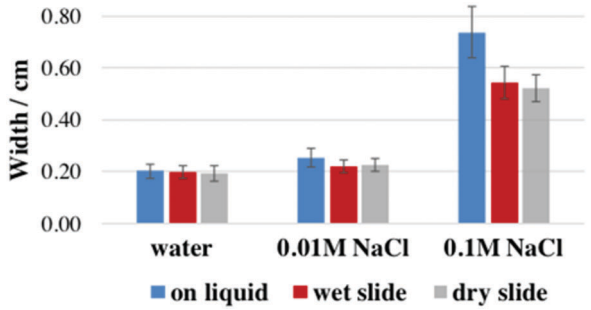

Fig. 9 Debye ring width, w of 915 nm diameter particle 2DPC at different stages of fabrication. 2DPC were fabricated by self-assembly of 915 nm PS particles on pure water, 0.01 M NaCl and 0.1 M NaCl. Error bars represent one standard deviation.

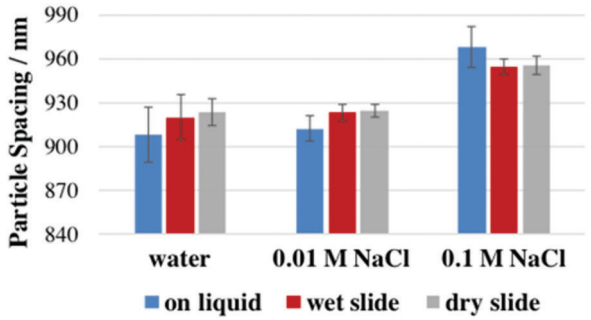

Fig. 10 Dependence of 2DPC particle spacings for 915 nm diameter particle 2DPC at different stages of fabrication. The Debye ring was measured for a 2DPC at the air–water interface of the crystallization dish (on liquid), at the air–water interface after the 2DPC and a thin water layer are transferred to a slide (wet slide), and after the 2DPC is dried on the slide (dry slide). 2DPC were fabricated by self-assembly of 915 nm PS particles on pure water, and in the presence of 0.01 M NaCl and 0.1 M NaCl. Error bars represent one standard deviation.

dependence for the Debye ring width of the 915 nm diameter 2DPC at the air–water interface of pure water, 0.01 M NaCl, and 0.1 M NaCl. The calculated particle spacings of these 2DPC samples are shown in Fig. 10.

With the exception of the 0.1 M NaCl samples, the Debye ring widths are the same for the 2DPC at the air–water interface, on the wet slide, and when dried on the slide, indicating that the 2DPC transfer to the slide, and drying has little impact on the array ordering. The Debye ring width of the 2DPC at the air–water interface of the 0.1 M NaCl samples may be slightly larger than the Debye ring width after transfer to the slide.

At 0.1 M NaCl concentrations, the particles spread from the needle tip increasingly disperse into the bulk water, increasing the turbidity of the water subphase. This turbidity partially obscures the diffuse Debye ring and makes it more difficult to measure its width. However, it is clear that the Debye ring widths of the 0.1 M NaCl samples are at least 2× greater than the widths of the 2DPC samples fabricated at lower salt concentrations.

The 2DPC particle spacing, a does not significantly change upon 2DPC transfer to the slide and the subsequent 2DPC drying. The 2DPC particle spacing at the air–water interface is very close to that found for the 2DPC on the wet and dried glass

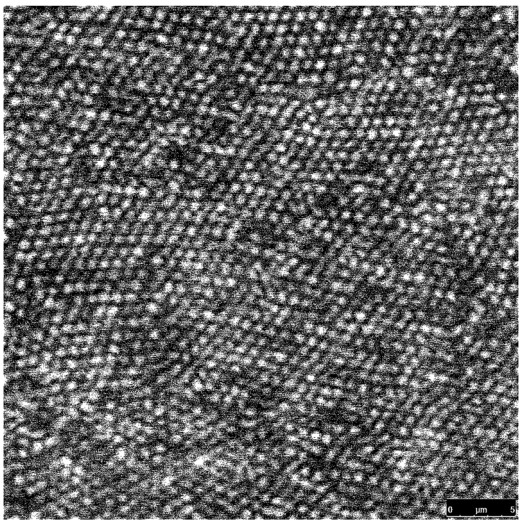

Fig. 11 Confocal microscope image of 915 nm particles at the air–water interface fabricated using the NTF method. The levels, thresholds, and sharpness in the image were edited using GIMP software so that the particles are clearly visible.

slides; these calculated particle spacings are roughly equal to the particle diameter when the 2DPC is well ordered. Thus, the NTF method produces self-assembled, highly ordered, hexagonal close packed (hcp) particle array monolayers at the air–water interface. These results are confirmed by confocal microscope imaging of the 915 nm 2DPC at the air–water interface, shown in Fig. 11. These results are significant because it shows that highly ordered close-packed 2DPC can be straight-forwardly fabricated at the air–water interface and transferred to substrates without disrupting 2DPC ordering or particle spacing.

It was recently proposed for the analogous micro-propulsive injection method[10] and other methods[21,48] that capillary attractive interactions between particles during water evaporation play a significant role in formation of the close packed structure. We believe we have shown that for the NTF method immersion capillary forces described by Kralchevsky and Nagayama[48] do not play a significant role in the formation of the close packed structure. The close packed particle array structure is present at the interface.

In a Langmuir–Blodgett trough, close packed hexagonal arrays are formed by compressing the monolayer to the close packed particle spacing after the particles are spread on the water surface.[49] This requires large amounts of sample and instrumentation that controls barrier movement and monitors the surface pressure. The NTF method is an improvement on the commonly used Langmuir–Blodgett method because it is faster, eliminates expensive instrumentation, avoids compression of the monolayer, and uses less sample.

Electrostatic interactions of charged particles at the air–water interface

The electrostatic interactions of charged colloidal particles at the air–water interface are different than the interactions of charged colloidal particles dispersed in solution. Interfacial particles are

partially exposed to water so that only the charged groups on the water exposed particle surface can dissociate.[50,51] The asymmetric ion cloud of the particle creates a dipole moment normal to the air–water interface.[19,52] Thus, the electrostatic repulsive interaction potential, ψ_{ES} (eqn (6)) of charged interfacial particles has contributions from the screened-Coulomb repulsions (first term of eqn (6)) and dipole–dipole repulsions (second term of eqn (6)).[53,54]

$$\psi_{ES} = \frac{2q^2\varepsilon^2}{s\varepsilon(\varepsilon^2-1)}\exp^{-\frac{s}{\mathcal{L}_D}} + 2\left(\frac{q\mathcal{L}_D}{\varepsilon}\right)^2 s^{-3} \quad (6)$$

where s is the distance between particle surfaces, q is the particle charge, $\mathcal{L}_D$ is the Debye screening length, and ε is the average of the air and water dielectric constants.

The screened-Coulomb repulsions decay rapidly with distance away from the particle. This short-range interaction dominates ψ_{ES} when the separation between particles is small. The dipole–dipole repulsions are long range interactions that dominate the potential when distances between particles are large.[53] These long range repulsive forces have been experimentally observed,[43,55] theoretically derived,[53] and modeled[56] for charged particles at the air–water or air–oil interface. If the particles are not constrained to a small finite surface area, the dipole–dipole repulsions will create hexagonal particle arrays with spacings larger than the particle diameter.[55]

The electrostatic interaction potential between particles decreases exponentially with distance between particles. The decay rate of the electrostatic interactions increases at higher salt concentrations. The particle surface charges electrostatically interact with ions in solution creating the electric double layer in the electrolyte solution surrounding the particle. Increasing the ion concentration in solution more effectively screens the electrostatic repulsive forces between the ionic interfacial particles and their electric double layers. The electric double layer thickness is roughly given by the Debye length, $\mathcal{L}_D(\text{nm}) = \left(\left(2000e^2N_A[\text{NaCl}]\right)/\left(\varepsilon_o\varepsilon_w kT\right)\right)^{1/2}$ for a 1:1 electrolyte.[57–59] The double layer thickness decreases with increasing salt concentration.

The Debye length of charged particles in electrolyte solutions decreases monotonically with increasing salt concentration. $\mathcal{L}_D$ is 966 nm for particles in pure water (ion concentration 10^{-7} M), 9.7 nm in 0.001 M NaCl, 3.1 nm in 0.01 M NaCl, 0.97 nm in 0.1 M NaCl, and 0.31 nm in 1 M NaCl. Accordingly, it is expected that the electrostatic repulsive interaction potential will monotonically decrease as salt concentration increases, which should have negative consequences on 2DPC ordering. Despite the seemingly straight forward relationship between salt concentration and the Debye screening length, both the Debye ring measurements and order parameter calculations show that 2DPC close packed self-assembly and ordering is not impeded by low salt concentrations using the NTF method. In contrast, at NaCl concentrations exceeding 0.01 M NaCl there is a dramatically increased disorder, indicating there is a mechanism counter-balancing the decrease in ψ_{ES} caused by decreasing $\mathcal{L}_D$.

Mechanism of self assembly for close packed particles arrays at the air water interface

The charged particles dispersed in a water/propanol mixture flow onto the air–water interface from the needle tip due to the large surface tension gradient between the particle dispersion and the water surface.[23,34,60] The interfacial particles are transported *via* Marangoni flow across the water surface towards interfacial areas with the highest surface tension. Marangoni flow induces the in-plane packing of the particles against the walls of the circular crystallization dish. The particles fill the water surface moving inward from the walls of the dish. This packing force thrusts the particles together so that particles order into a close packed hexagonal array.

The packing force is counter-balanced by the strong electrostatic repulsions that prevent interparticle adhesion and aggregation of random clusters. The electrostatic repulsive interactions between highly charged particles on a pure water surface are larger than the combined attractive van der Waals interactions and the packing force. The interparticle surface spacings of 2DPC fabricated by the NTF method are small, therefore the screened-Coulomb repulsions are the dominant electrostatic force driving self-assembly of ordered 2DPC.

The particle mobility gained from the strong electrostatic repulsions give the individual particles time to anneal. Here the term anneal is used to describe the process where individual particles are capable of jiggling around each other on the crowded air–water interface to form the ordered hexagonal 2D particle array with a minimum energy structure.

At low and modest salt concentrations, the particles do not contact one another. The separated particles have a thin water layer between them which lubricates the particle annealing process, to form 2D colloidal crystals. At higher salt concentrations, the electrostatic repulsive interactions are weak and particles approach one another more closely. This increases the probability of interparticle adhesion caused by van der Waals forces where they collapse into their primary minimum, or they suffer polymer entanglements that could also lead to particle sticking. This stabilizes disorder by slowing or preventing annealing. Disordered 2D arrays form with increased average interparticle spacing and larger Debye ring widths (Fig. 6 and 7). This disorder stems from the aggregation of randomly ordered particle clusters.

The unexpected behaviour of the 2DPC ordering as the ionic strength increases appears to result from adsorption of Cl^- onto the polystyrene particles as is independently shown by the salt concentration dependence of the Zeta potential, ξ shown in Fig. 12. Chloride anions have been previously shown to adsorb to anionic polystyrene surfaces, increasing the electrophoretic mobility of the particles up to a critical salt concentration.[61,62] Increasing the salt concentration further, decreases the electrophoretic mobility due to the collapse of the electric double layer in the high ionic strength solution.

The increase in ξ (more negative) for anionic polystyrene colloids at low concentrations of NaCl salt results from chloride adsorption.[61,62] ξ reaches a minimum at a NaCl concentration that is consistent with the critical salt concentration, C^* determined from the ordering results. At larger salt concentrations,

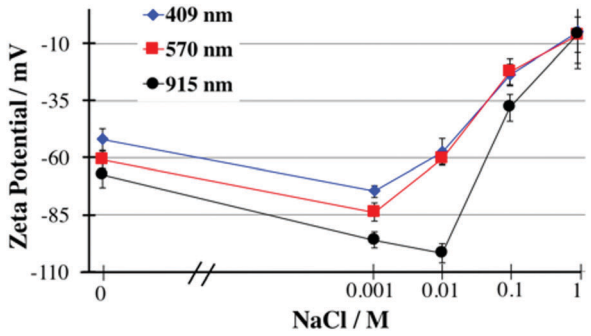

Fig. 12 Zeta-potentials, ξ (mV) for 409, 570, and 915 nm diameter anionic polystyrene particles in solutions as a function of NaCl concentration. Error bars indicate one standard deviation.

ξ decreases sharply (less negative) due to compression of the diffuse electric double layer and counter-ion screening. The critical salt concentration, C^* at which this transition occurs is dependent on particle diameter. Again, we find the same C^* for a certain particle diameter in the zeta-potential data as in the Debye ring diffraction and order parameter results.

The similarity between the zeta potential, Debye ring measurement, and calculated order parameter results suggests adsorption of Chloride ions onto the polystyrene surface increases the particle anionic surface charge significantly and counteracts the decreasing $\mathcal{L}_D$. Chloride ions adsorbed to the polystyrene surface act as potential determining ions to increase interparticle electrostatic repulsions; this results in better annealing and therefore better ordering of the self-assembled 2DPC.

Conclusions

We have shown that utilization of Debye ring measurements is a viable method for monitoring 2DPC ordering for colloidal particle arrays having diameters roughly the size of the wavelengths of visible light. This method could be extended to larger or smaller particles by utilizing infrared or UV light and a detector. The Debye ring thickness is a reliable indicator of 2DPC order because 2DPC disorder creates larger average particle spacings that decrease the Debye ring inner diameter. Conclusions on 2DPC ordering drawn from Debye ring measurements are consistent with the order parameter found by analysing SEM micrographs of the 2DPC.

Using the Debye ring method, we show the NTF method for self-assembly of 2DPC produces highly ordered hexagonal close packed (hcp) monolayers of colloidal particles (diameters = 409, 570, and 915 nm). While investigating the relationship between 2DPC ordering and Debye ring diffraction, we discovered that disorder in the 2DPC does not monotonically increase as salt concentration increases. This behaviour is attributed to chloride anion adsorption to the particle surface. The behaviour of the zeta potential of particles in salt solutions is analogous to the 2DPC ordering results for 2DPC fabricated on salt solutions. This leads to the conclusion that chloride adsorption increases the particle surface charge which compensates for the decreasing Debye length at low or moderate salt concentrations.

Conflicts of interest

There are no conflicts to declare.

Acknowledgements

This work was funded by the Defence Threat Reduction Agency under grant HDTRA1-15-1-0038. We acknowledge Tom Harper and the University of Pittsburgh Department of Biological Sciences for providing instrumentation and assistance in obtaining the confocal microscope images. We thank Clay Colonna (http://www.claycolonna.com) for his assistance in cutting and formatting the video provided in the ESI.†

Notes and references

1 D. W. Prather, A. Sharkawy, S. Shi, J. Murakowski and G. Schneider, *Photonic Crystals, Theory, Applications and Fabrication*, Wiley Publishing, 2009.
2 M. V. Rybin, A. B. Khanikaev, M. Inoue, K. B. Samusev, M. J. Steel, G. Yushin and M. F. Limonov, *Phys. Rev. Lett.*, 2009, **103**, 023901.
3 B. van Duffel, R. H. A. Ras, F. C. De Schryver and R. A. Schoonheydt, *J. Mater. Chem.*, 2001, **11**, 3333–3336.
4 H. N. Chapman, *et al.*, *Nature*, 2011, **470**, 73–77.
5 V. Elser and C. L. Henley, *Phys. Rev. Lett.*, 1985, **55**, 2883–2886.
6 N. K. Alexander Tikhonov, J.-T. Zhang, L. Wang and S. A. Asher, *J. Nanophotonics*, 2012, **6**, 063509.
7 N. L. Smith, Z. Hong and S. A. Asher, *Analyst*, 2014, **139**, 6379–6386.
8 J.-T. Zhang, L. Wang, J. Luo, A. Tikhonov, N. Kornienko and S. A. Asher, *J. Am. Chem. Soc.*, 2011, **133**, 9152–9155.
9 Z. Cai, N. L. Smith, J.-T. Zhang and S. A. Asher, *Anal. Chem.*, 2015, **87**, 5013–5025.
10 P. Gao, J. He, S. Zhou, X. Yang, S. Li, J. Sheng, D. Wang, T. Yu, J. Ye and Y. Cui, *Nano Lett.*, 2015, **15**, 4591–4598.
11 M. S. Branham, W.-C. Hsu, S. Yerci, J. Loomis, S. V. Boriskina, B. R. Hoard, S. E. Han and G. Chen, *Adv. Mater.*, 2015, **27**, 2182–2188.
12 M. Karg, T. A. F. König, M. Retsch, C. Stelling, P. M. Reichstein, T. Honold, M. Thelakkat and A. Fery, *Mater. Today*, 2015, **18**, 185–205.
13 S. Utech, K. Bley, J. Aizenberg and N. Vogel, *J. Mater. Chem. A*, 2016, **4**, 6853–6859.
14 J. Bravo, L. Zhai, Z. Wu, R. E. Cohen and M. F. Rubner, *Langmuir*, 2007, **23**, 7293–7298.
15 Y. Li, J. Zhang, S. Zhu, H. Dong, F. Jia, Z. Wang, Z. Sun, L. Zhang, Y. Li, H. Li, W. Xu and B. Yang, *Adv. Mater.*, 2009, **21**, 4731–4734.
16 M. D. Malinsky, K. L. Kelly, G. C. Schatz and R. P. Van Duyne, *J. Am. Chem. Soc.*, 2001, **123**, 1471–1482.
17 A. Das, J. Zhao, G. C. Schatz, S. G. Sligar and R. P. Van Duyne, *Anal. Chem.*, 2009, **81**, 3754–3759.
18 K. Shinotsuka, Y. Kajita, K. Hongo and Y. Hatta, *Langmuir*, 2015, **31**, 11452–11457.

19 N. Vogel, C. K. Weiss and K. Landfester, *Soft Matter*, 2012, **8**, 4044–4061.
20 J. Zhang, Y. Li, X. Zhang and B. Yang, *Adv. Mater.*, 2010, **22**, 4249–4269.
21 V. Lotito and T. Zambelli, *Adv. Colloid Interface Sci.*, 2017, **246**, 217–274.
22 X. N. Xie, H. J. Chung, C. H. Sow and A. T. S. Wee, *Mater. Sci. Eng., R*, 2006, **54**, 1–48.
23 J.-T. Zhang, L. Wang, D. N. Lamont, S. S. Velankar and S. A. Asher, *Angew. Chem., Int. Ed.*, 2012, **51**, 6117–6120.
24 T. Ogi, L. B. Modesto-Lopez, F. Iskandar and K. Okuyama, *Colloids Surf., A*, 2007, **297**, 71–78.
25 D. Truzzolillo, H. Sharaf, U. Jonas, B. Loppinet and D. Vlassopoulos, *Langmuir*, 2016, **32**, 6956–6966.
26 J. Y. Kim, S. J. Kwon, J.-B. Chang, C. A. Ross, T. A. Hatton and F. Stellacci, *Nano Lett.*, 2016, **16**, 1352–1358.
27 M. Hu, S. Chujo, H. Nishikawa, Y. Yamaguchi and T. Okubo, *J. Nanopart. Res.*, 2004, **6**, 479–487.
28 C.-C. Ho, P.-Y. Chen, K.-H. Lin, W.-T. Juan and W.-L. Lee, *ACS Appl. Mater. Interfaces*, 2011, **3**, 204–208.
29 M. Retsch, Z. Zhou, S. Rivera, M. Kappl, X. S. Zhao, U. Jonas and Q. Li, *Macromol. Chem. Phys.*, 2009, **210**, 230–241.
30 T. Okubo, S. Chujo, S. Maenosono and Y. Yamaguchi, *J. Nanopart. Res.*, 2003, **5**, 111–117.
31 S. C. Rödner, P. Wedin and L. Bergström, *Langmuir*, 2002, **18**, 9327–9333.
32 M. Grzelczak, J. Vermant, E. M. Furst and L. M. Liz-Marzán, *ACS Nano*, 2010, **4**, 3591–3605.
33 N. V. Minh, N. T. Hue, N. T. H. Lien and C. M. Hoang, *Electron. Mater. Lett.*, 2017, DOI: 10.1007/s13391-017-6389-x.
34 J.-T. Zhang, L. Wang, X. Chao, S. S. Velankar and S. A. Asher, *J. Mater. Chem. C*, 2013, **1**, 6099–6102.
35 F. Zhang, L. Cao and W. Yang, *Macromol. Chem. Phys.*, 2010, **211**, 744–751.
36 C. E. Reese and S. A. Asher, *J. Colloid Interface Sci.*, 2002, **248**, 41–46.
37 J.-T. Zhang, X. Chao, X. Liu and S. A. Asher, *Chem. Commun.*, 2013, **49**, 6337–6339.
38 J. J. Bohn, M. Ben-Moshe, A. Tikhonov, D. Qu, D. N. Lamont and S. A. Asher, *J. Colloid Interface Sci.*, 2010, **344**, 298–307.
39 R. Rengarajan, D. Mittleman, C. Rich and V. Colvin, *Phys. Rev. E: Stat., Nonlinear, Soft Matter Phys.*, 2005, **71**, 016615.
40 J.-T. Zhang, X. Chao and S. A. Asher, *J. Am. Chem. Soc.*, 2013, **135**, 11397–11401.
41 F. Xue, S. A. Asher, Z. Meng, F. Wang, W. Lu, M. Xue and F. Qi, *RSC Adv.*, 2015, **5**, 18939–18944.
42 C. Weitenberg, P. Schauß, T. Fukuhara, M. Cheneau, M. Endres, I. Bloch and S. Kuhr, *Phys. Rev. Lett.*, 2011, **106**, 215301.
43 P. Pieranski, *Phys. Rev. Lett.*, 1980, **45**, 569–572.
44 M. Schmudde, C. Grunewald, C. Goroncy, C. N. Noufele, B. Stein, T. Risse and C. Graf, *ACS Nano*, 2016, **10**, 3525–3535.
45 V. Lotito and T. Zambelli, *Langmuir*, 2016, **32**, 9582–9590.
46 F. Reincke, W. K. Kegel, H. Zhang, M. Nolte, D. Wang, D. Vanmaekelbergh and H. Mohwald, *Phys. Chem. Chem. Phys.*, 2006, **8**, 3828–3835.
47 H. Yoshida, K. Ito and N. Ise, *J. Chem. Soc., Faraday Trans.*, 1991, **87**, 371–378.
48 P. A. Kralchevsky and K. Nagayama, *Langmuir*, 1994, **10**, 23–36.
49 M. Bardosova, M. E. Pemble, I. M. Povey and R. H. Tredgold, *Adv. Mater.*, 2010, **22**, 3104–3124.
50 V. N. Paunov, *Langmuir*, 2003, **19**, 7970–7976.
51 R. Aveyard, J. H. Clint, D. Nees and V. N. Paunov, *Langmuir*, 2000, **16**, 1969–1979.
52 G. V. Bossa, K. Bohinc, M. A. Brown and S. May, *J. Phys. Chem. B*, 2016, **120**, 6278–6285.
53 A. J. Hurd, *J. Phys. A: Math. Gen.*, 1985, **18**, L1055.
54 S. Wu, A. Nikolov and D. Wasan, *Can. J. Chem. Eng.*, 2007, **85**, 562–569.
55 M. G. Nikolaides, A. R. Bausch, M. F. Hsu, A. D. Dinsmore, M. P. Brenner, C. Gay and D. A. Weitz, *Nature*, 2002, **420**, 299–301.
56 M. Girotto, A. P. dos Santos and Y. Levin, *J. Phys. Chem. B*, 2016, **120**, 5817–5822.
57 T. Okubo, *Acc. Chem. Res.*, 1988, **21**, 281–286.
58 R. J. Hunter, *Zeta Potential in Colloid Science*, Academic Press Inc, New York, New York, 1981.
59 P. C. Hiemenz, *Principles of Colloid and Surface Chemistry*, Marcel Dekker, Inc, New York, 2nd edn, 1986.
60 L. Dong and D. Johnson, *Langmuir*, 2003, **19**, 10205–10209.
61 M. Elimelech and C. R. O'Melia, *Colloids Surf.*, 1990, **44**, 165–178.
62 C. M. Ma, F. J. Micale, M. S. El-Aasser and J. W. Vanderhoff, *Emulsion Polymers and Emulsion Polymerization*, American Chemical Society, 1981, vol. 165, ch. 15, pp. 251–262.

